Quantum-orbit analysis of the generation of a high-ellipticity attosecond pulse with circular-elliptical bichromatic laser fields

MuFeng Zhu,[1,2] XuanYang Lai,[1,*] LinQiang Hua,[1] and XiaoJun Liu[1,†]
[1]*State Key Laboratory of Magnetic Resonance and Atomic and Molecular Physics, Innovation Academy for Precision Measurement Science and Technology, Chinese Academy of Sciences, Wuhan 430071, China*
[2]*School of Physical Sciences, University of Chinese Academy of Sciences, Beijing 100049, China*

(Received 20 June 2023; accepted 12 September 2023; published 6 October 2023)

We study attosecond pulses synthesized from high-order harmonic generation (HHG) under different circular-elliptical bichromatic laser fields by numerically solving the time-dependent Schrödinger equation. For ω-3ω bichromatic laser fields, the ellipticity of parts of the elliptically polarized attosecond pulse train (APT) in each optical cycle will first approach unity and then decrease as the ellipticity of the 3ω field decreases. However, for the ω-2ω bichromatic laser field, the ellipticity of the APT remains small when the ellipticity of the 2ω field decreases. Our result is well reproduced in terms of quantum-orbit theory. By analyzing the quantum orbits, the underlying physics for the generation of the nearly circularly polarized attosecond pulse with the ω-3ω circular-elliptical bichromatic laser field is revealed. Our work provides a simple method to obtain highly elliptically polarized attosecond pulses from HHG.

DOI: 10.1103/PhysRevA.108.043106

I. INTRODUCTION

Attosecond pulses are a powerful tool to probe the ultrafast dynamics of an electron in an atom or a molecule [1–5]. An efficient way to synthesize the attosecond pulse is by using high-order harmonic generation (HHG) [6–10], which is an extremely nonlinear frequency conversion process and can be understood with a simple three-step model [11,12]. During the past few decades, great progress in the generation of attosecond pulses with HHG has been achieved [13–16]. For example, an attosecond pulse with a pulse duration of 53 as was obtained in experiment [15]. Usually, the attosecond pulse synthesized with HHG is linearly polarized [17–19]. The reason is that the harmonic is generated from the interaction of an atom or a molecule with a linearly polarized laser field, while for a circularly polarized laser field, the harmonic emission is greatly suppressed according to the three-step model. With the development of attosecond science, it has been found that circularly or highly elliptically polarized attosecond pulses have many important applications, such as the detection of the chirality of atoms and molecules [20–25] and the measurement of magnetic circular dichroism, time-resolved magnetization dynamics, and spin currents [26–30]. Therefore, the way to obtain a highly elliptically polarized attosecond pulse with HHG has attracted great attention.

Recently, some methods were proposed to obtain circularly or highly elliptically polarized attosecond pulses from HHG. For example, by using a bicircular laser field, pairs of completely circularly polarized harmonics with opposite helicity can be obtained [31–43]. By adjusting the relative intensity ratio of the bicircular laser field, either the right- or left-circularly polarized harmonics are preferentially selected, and accordingly, a synthesized attosecond pulse with high ellipticity is generated [44–46]. Based on this scheme, it has been shown that the ellipticity of the attosecond pulse train (APT) can reach 0.77 [45]. To further increase the ellipticity of an attosecond pulse, a scheme with a three-color laser field, including an orthogonally polarized two-color laser field and an infrared (IR) field, was proposed to generate a nearly circularly polarized attosecond pulse [47], in which the IR field offers extra angular momentum to the return electron. However, in this scheme, it is difficult to manipulate the three-color laser fields in experiment. On the other hand, an alternative method with an available unidirectionally rotating laser field was proposed to produce nearly circularly polarized attosecond pulses from aligned CO molecules [48]. However, this method strongly depends on the ideal molecular orientation. For example, if the orientation degree of the molecule is about 0.9, the ellipticity of the generated attosecond pulse decreases to 0.85. Thus, it is still difficult to produce a nearly circularly polarized attosecond pulse with this scheme in experiment. Note that a recent study demonstrated that by using a linearly polarized infrared pulse in the presence of an XUV pulse with orthogonal polarization [49], the polarization properties of HHG from an atom can be controlled by separating the contribution of amplitudes associated with short trajectories. This approach holds potential for generating highly elliptically polarized attosecond pulses. However, it remains uncertain whether this method can effectively produce a nearly circularly polarized attosecond pulse.

Interestingly, it was recently found [50] that by decreasing the ellipticity of the bicircular laser fields, pairs of harmonics in the spectra were no longer circularly polarized. Furthermore, the absolute values of the ellipticity for ad-

*xylai@wipm.ac.cn
†xjliu@wipm.ac.cn

jacent harmonics were found to be unequal. Such changes in the harmonic characteristics may potentially impact the ellipticity of synthesized attosecond pulses. A fingerprint of a highly elliptical attosecond pulse in an APT under a circular-elliptical bichromatic laser field can be found in time-dependent Schrödinger equation (TDSE) simulations [51,52]. However, how the circular-elliptical bichromatic laser field affects the ellipticity of the attosecond pulse and whether this scheme depends on the frequency combination of the bichromatic laser field, e.g., the ω-3ω field or the ω-2ω field, are still unknown.

In this work, we study the generation of attosecond pulses from HHG of an atom under the ω-3ω and ω-2ω circular-elliptical bichromatic laser fields by numerically solving the TDSE. Our TDSE simulation shows that for the ω-3ω bichromatic laser field, the ellipticity of parts of the elliptically polarized APT in each optical cycle of the fundamental laser field will increase with the decrease of the ellipticity of the 3ω field, ultimately reaching a point where a nearly circularly polarized attosecond pulse can be achieved. However, a further decrease in the ellipticity of the 3ω field subsequently results in a decrease in the ellipticity of the APT. However, for the ω-2ω bichromatic laser field, the ellipticity of the APT remains small when the ellipticity of the 2ω field decreases. The TDSE simulation is well reproduced in terms of quantum-orbit theory, and through an analysis of the quantum orbits, the underlying physics of the generation of the nearly circularly polarized attosecond pulse with the ω-3ω circular-elliptical bichromatic laser field is revealed.

This paper is organized as follows. In Sec. II, we briefly introduce the TDSE and quantum-orbit theory. In Sec. III, we present the TDSE simulations of the HHG spectra and the corresponding attosecond pulses. Subsequently, the HHG spectra are reproduced with the quantum-orbit theory, and the underlying physics of the generation of the highly elliptically polarized attosecond pulse is revealed. Finally, in Sec. IV, our conclusions are given. Atomic units are used unless stated otherwise.

II. THEORETICAL METHODS

A. TDSE method for HHG

HHG of an atom under a circular-elliptical bichromatic laser field is simulated by solving the three-dimensional TDSE in the velocity gauge,

$$i\frac{\partial}{\partial t}\Psi(\mathbf{r},t)=\left[-\frac{1}{2}\nabla^2+V(\mathbf{r})-i\mathbf{A}(t)\cdot\nabla\right]\Psi(\mathbf{r},t), \quad (1)$$

where $V(\mathbf{r})$ is the Coulomb potential of the atom and $\mathbf{A}(t)$ is the vector potential of the laser field in the dipole approximation [i.e., the electric field is $\mathbf{E}(t)=-\partial_t\mathbf{A}(t)$]. The vector potentials in the x and y directions are given by

$$\begin{aligned}A_x(t)&=f(t)\left[-\frac{E_1}{\sqrt{2}\omega}\sin(\omega t)-\frac{E_2}{\sqrt{1+\xi^2}n\omega}\sin(n\omega t)\right]\hat{e}_x,\\ A_y(t)&=f(t)\left[\frac{E_1}{\sqrt{2}\omega}\cos(\omega t)-\xi\frac{E_2}{\sqrt{1+\xi^2}n\omega}\cos(n\omega t)\right]\hat{e}_y,\end{aligned} \quad (2)$$

where $n=2$ and 3 for the ω-2ω and ω-3ω circular-elliptical bichromatic laser fields, respectively, ξ is the ellipticity of the 3ω or 2ω laser field, and $f(t)$ is the envelope function. In our simulation, the laser pulse has a six-cycle flat-top part and two-cycle $\sin^2$-shape up and down rampings. The three-dimensional TDSE is solved using the freely available software QPROP [53]. In this work, we will take the He atom as an example with the Coulomb potential [54] $V(r)=-(Z_c+a_1e^{-a_2r}+a_3re^{-a_4r}+a_5e^{-a_6r})/r$, where the coefficients are $Z_c=1$, $a_1=1.231$, $a_2=0.662$, $a_3=-1.325$, $a_4=1.236$, $a_5=-0.231$, and $a_6=0.48$.

After the time-dependent electronic wave function is obtained, the corresponding HHG spectra in the x and y directions are given by [55]

$$\begin{aligned}P_x(\omega)&=\left|\frac{1}{t_f-t_i}\frac{1}{\omega^2}\int_{t_i}^{t_f}d_{ax}(t)e^{-i\omega t}dt\right|^2,\\ P_y(\omega)&=\left|\frac{1}{t_f-t_i}\frac{1}{\omega^2}\int_{t_i}^{t_f}d_{ay}(t)e^{-i\omega t}dt\right|^2,\end{aligned} \quad (3)$$

where the time-dependent induced dipole accelerations are written as [56]

$$\begin{aligned}d_{ax}(t)&=\langle\Psi(x,y,t)|-\frac{\partial V(x,y)}{\partial x}+E_x(t)|\Psi(x,y,t)\rangle,\\ d_{ay}(t)&=\langle\Psi(x,y,t)|-\frac{\partial V(x,y)}{\partial y}+E_y(t)|\Psi(x,y,t)\rangle.\end{aligned} \quad (4)$$

Accordingly, the total HHG power spectra can be expressed as $P(\omega)=\sqrt{P_x(\omega)+P_y(\omega)}$.

To synthesize the attosecond pulse with HHG, a group of the harmonics is selected. The corresponding electric-field vectors of the attosecond pulse in the x and y directions are given by [57]

$$E_{ax}(t)=\sum_q a_{qx}e^{iq\omega t},\quad E_{ay}(t)=\sum_q a_{qy}e^{iq\omega t}, \quad (5)$$

where $a_{qx}=\int d_{ax}(t)e^{-iq\omega t}dt$, $a_{qy}=\int d_{ay}(t)e^{-iq\omega t}dt$, and q is the harmonic order.

B. Quantum-orbit theory within the strong-field approximation

To understand the TDSE results, quantum-orbit theory within the strong-field approximation (SFA) [58] is employed to simulate the HHG. The intensity of the qth harmonic is given by [43,46,59]

$$I_q=\frac{(q\omega)^4}{2\pi c^3}|\mathbf{T}_q|^2, \quad (6)$$

where $\mathbf{T}_q=\int_0^T\frac{dt}{T}e^{iq\omega t}\sum_m\boldsymbol{d}_m(t)$, m is the magnetic quantum number, and $d_m(t)$ is the time-dependent dipole moment. In this work, the dipole moment is written as [43,46,60]

$$\begin{aligned}\boldsymbol{d}_m(t)=-i\int d^3\boldsymbol{p}\int_{-\infty}^{t}dt_0\langle\boldsymbol{p}+\boldsymbol{A}(t_0)|\boldsymbol{r}\cdot\boldsymbol{E}(t_0)|\Phi_{lm}\rangle\\ \times e^{iS(\boldsymbol{p},t,t_0)}\langle\Phi_{lm}|\boldsymbol{r}|\boldsymbol{p}+\boldsymbol{A}(t)\rangle,\end{aligned} \quad (7)$$

where $\boldsymbol{p}$ is the drift momentum of the electron between the ionization time t_0 and recombination time t and $S(\boldsymbol{p},t,t_0)=-I_p\tau-\int_{t_0}^{t}dt'[\boldsymbol{q}+\boldsymbol{A}(t')]^2/2$ is the quasiclassical action, with $\tau=t-t_0$ and I_p being the ionization potential. The ground-state atomic wave function Φ_{lm} is written as a linear

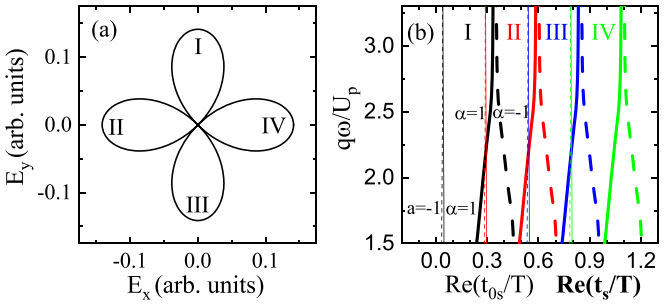

FIG. 1. (a) The Lissajous curve of the electrical field of the ω-3ω bicircular laser field. The total laser intensity is 7×10^{14} W/cm^2, and the fundamental frequency ω is 0.057 a.u. (b) The solutions of t_{0s} (thin lines) and t_s (thick lines) for quantum orbits from the four segments of the laser field, where U_p is the ponderomotive energy and indices $\alpha = \pm 1$ represent the short orbits and long orbits of the ionized electron, which are marked by the solid lines and dashed lines, respectively.

combination of the asymptotic wave functions [61–66]: $\Phi_{lm} = Ar^{\nu-1}\exp(-\kappa r)Y_{lm}(\boldsymbol{r})$, where $\nu = Z/\kappa$, $\kappa = \sqrt{2I_p}$, Z is the charge of the atomic residue, and l is the orbital quantum number. The values of A for different gases are tabulated in [61]. For the ground state of the He atom, $l = m = 0$, and $A = 2.87$.

To solve Eqs. (6) and (7), the saddle-point method is used, and the corresponding harmonic amplitude is approximately given by [43,59]

$$T_q^j = b\sum_s \frac{[\boldsymbol{Q}_{0s}/(i\kappa)]^l}{[i(t_s - t_{0s})]^{3/2}}\left(\frac{2i}{S''_{0s}}\right)^{\nu+1/2}\left(\frac{2i}{S''_s}\right)^{1/2} e^{iS_s} \times \sum_m \langle \Phi_{lm}|j|\boldsymbol{Q}_s\rangle Y_{lm}(\boldsymbol{Q}_{0s}), \tag{8}$$

where s denotes the different quantum orbits, $b = \pi^2 A\kappa^\nu \nu\Gamma(\nu/2)/T$, $j = x$ or y, $\boldsymbol{Q}_{0s} = \boldsymbol{p} + \boldsymbol{A}(t_0)$, $\boldsymbol{Q}_s = \boldsymbol{p} + \boldsymbol{A}(t_s)$, the action of each quantum orbit $S_s = S(\boldsymbol{p}, t_s, t_{0s}) + q\omega t_s$, and t_{0s} and t_s represent the ionization and recombination times of the quantum orbit, respectively. The quantum orbits are obtained by solving the saddle-point equations [60–62,67,68]

$$[\boldsymbol{p} + \boldsymbol{A}(t_{0s})]^2 = -2I_p, \tag{9a}$$

$$(t_s - t_{0s})\boldsymbol{p} = -\int_{t_{0s}}^{t_s} dt' \boldsymbol{A}(t'), \tag{9b}$$

$$[\boldsymbol{p} + \boldsymbol{A}(t_s)]^2 = 2(q\omega - I_p). \tag{9c}$$

Because the right-hand side of the first equation is negative, the solutions of t_{0s}, t_s, and $\boldsymbol{p}$ are complex. Figure 1 gives an example of the Lissajous curve and the solutions of t_{0s} and t_s for the ω-3ω bicircular laser field. It shows that there are four segments within one optical cycle of the fundamental laser field, and accordingly, there are four groups of the quantum orbits. On the other hand, for the ω-2ω bicircular laser field, the Lissajous curve of the electric field is a trefoil, and there are three groups of quantum orbits in one optical cycle of the fundamental laser field [45,61,69]. After the harmonic amplitudes are obtained according to Eq. (8), the attosecond pulses can be obtained by superposing a group of harmonics,

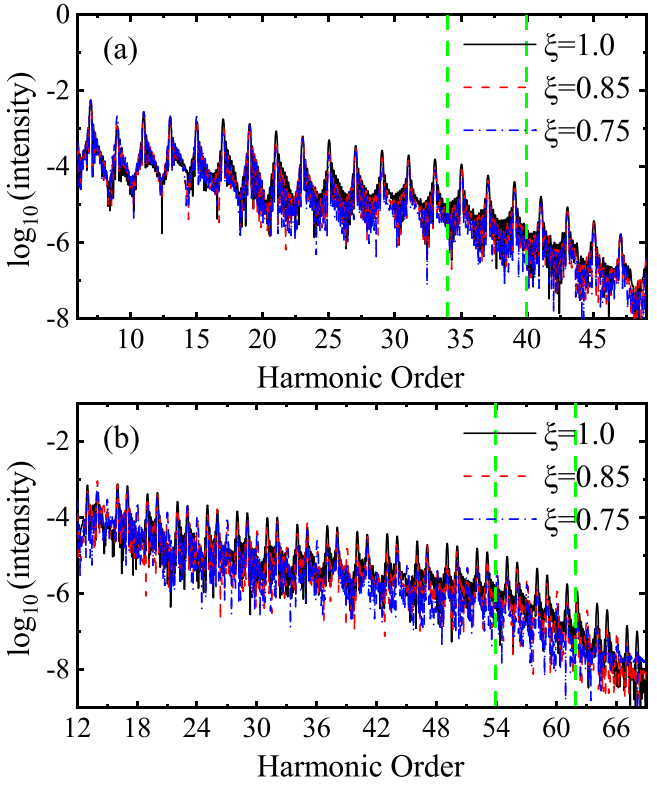

FIG. 2. TDSE-simulated HHG spectra of the He atom under (a) the ω-3ω and (b) the ω-2ω circular-elliptical bichromatic laser fields with different values of ξ. The region between the vertical green dashed lines denotes the selected harmonics for the generation of the APTs.

and the corresponding electric-field vectors of the attosecond pulses in the x and y directions are given by [43,69]

$$E_{ax}(t) = \sum_q q^2 T_q^x \exp(-iq\omega t),$$

$$E_{ay}(t) = \sum_q q^2 T_q^y \exp(-iq\omega t). \tag{10}$$

III. RESULTS AND DISCUSSION

In Fig. 2, we present the TDSE-simulated HHG spectra of a He atom under the ω-3ω and ω-2ω circular-elliptical bichromatic laser fields. The fundamental laser field has a wavelength of 800 nm, and the intensity ratio between the fundamental and additional fields is equal to 1, with a total intensity of 7×10^{14} W/cm^2. The TDSE simulation shows that only $(4q \pm 1)$th-order harmonics are emitted for the ω-3ω bicircular laser field (ξ =1), while they become $3q \pm 1$ for the ω-2ω bicircular laser field. Our results are consistent with previous calculations [26,40–44,70–72]. With the decrease in the ellipticity ξ of the 3ω and 2ω fields, the orders of the harmonic radiation remain the same for the ω-3ω laser field, but additional 3qth-order harmonics appear for the ω-2ω laser field. The reason is that for the ω-3ω circular-elliptical bichromatic laser field, the electric field has symmetry with the half cycle of the fundamental field when decreasing the ellipticity ξ of the 3ω field (see the discussion of Fig. 7

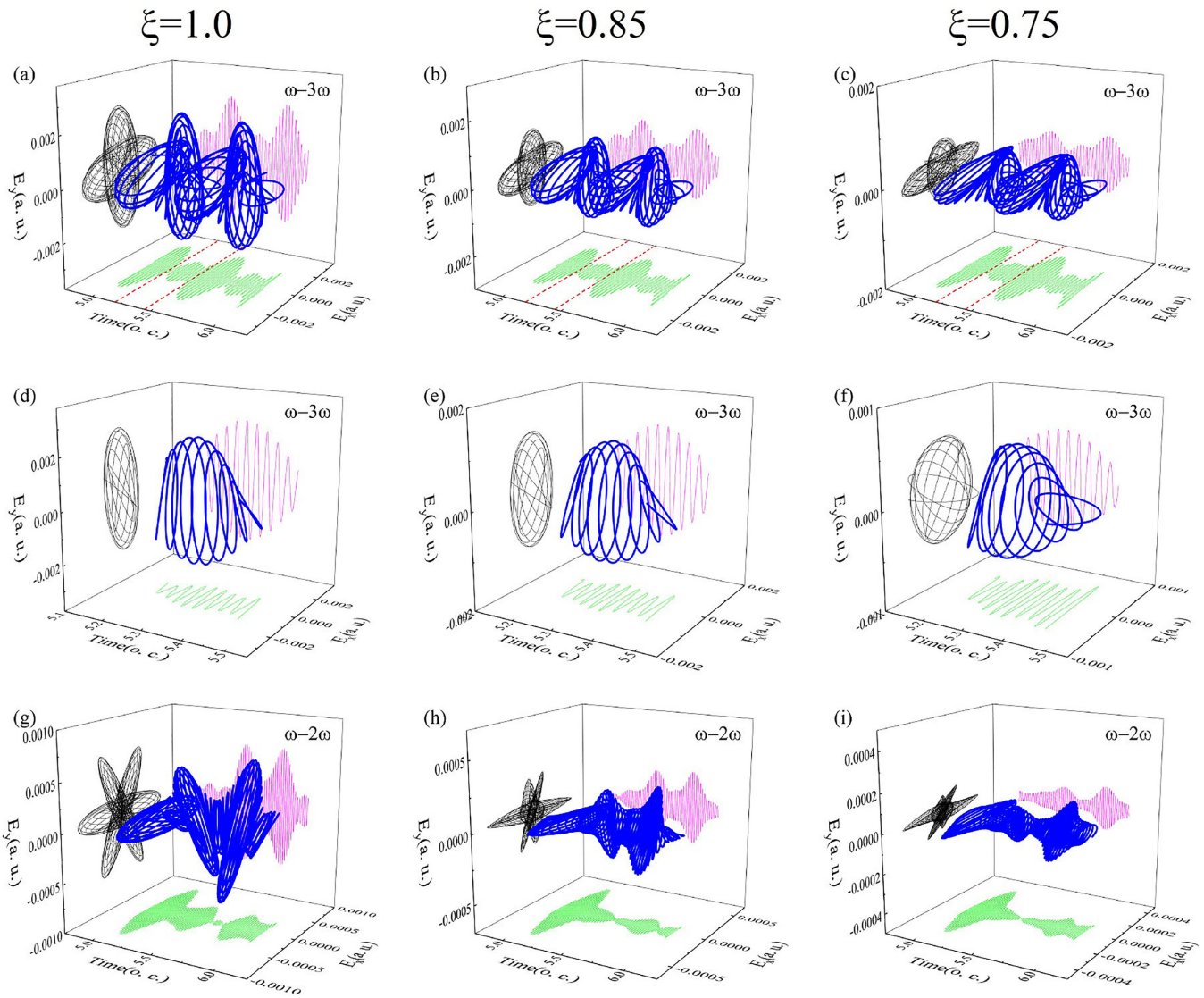

FIG. 3. (a)–(c) The APT synthesized with the 34th- to 40th-order harmonics from the He atom under the ω-3ω circular-elliptical bichromatic laser fields with different values of ξ. The electric vector of the APT is plotted by using the real part of Eq. (5). (d)–(f) Zoomed-in view of the attosecond pulses in the time window of the 5.2–5.45 optical cycle [marked by the red dashed lines in (a)–(c)]. (g)–(i) The APT synthesized with the 54th- to 62nd-order harmonics from the He atom under the ω-2ω circular-elliptical bichromatic laser fields with different values of ξ.

below), and accordingly, the $(2q \pm 1)$th-order harmonics are emitted, which coincides with the $(4q \pm 1)$th-order harmonics generated from the ω-3ω bicircular laser field. In contrast, for the ω-2ω bichromatic laser field, the symmetry of the laser field is completely destroyed when the ellipticity ξ of the 2ω field is changed (see the discussion of Fig. 8 below); thus, the additional $3q$th-order harmonics are emitted. In the following, we will mainly focus on the ellipticity of the APTs synthesized from the harmonics.

In Figs. 3(a)–3(c), we show the APTs synthesized with the harmonics near the cutoff region for the ω-3ω circular-elliptical bichromatic laser field with $\xi = 1.0$, 0.85, and 0.75, respectively. These plots clearly show that for the ω-3ω circular-elliptical bichromatic laser field, there are four attosecond bursts in one optical cycle whose polarization directions differ from each other by 90°. With the decrease in the ellipticity ξ of the 3ω field, the ellipticity of the first and third attosecond bursts decreases, while the ellipticity of the second and fourth attosecond bursts increases. To more clearly show the increase in the ellipticity of the attosecond bursts with the ellipticity of the 3ω field, the second attosecond burst in the specific temporal window of the 5.2-5.45 optical cycle of the fundamental pulse is shown in Figs. 3(d)–3(f). When $\xi = 0.75$, a nearly circularly polarized attosecond pulse with an ellipticity of $\chi \approx 0.99$ can be obtained, where $\chi = (|E_+|^2 - |E_-|^2)/(|E_+|^2 + |E_-|^2)$ and $E_\pm$ are the two helical components of the electric field of the APT in the time domain $E_\pm(t) = \mp[E_x(t) \pm iE_y(t)]/\sqrt{2}$ [44,45,52]. In order to better illustrate the variation in ellipticity of the attosecond pulse under the ω-3ω circular-elliptical bichromatic laser field, we present in Fig. 4 the maximum ellipticity of the attosecond pulse (synthesized using the 34th- to 40th-order harmonics) as a function of the ellipticity of the 3ω component. Interestingly, as the ellipticity of the 3ω component decreases, the ellipticity

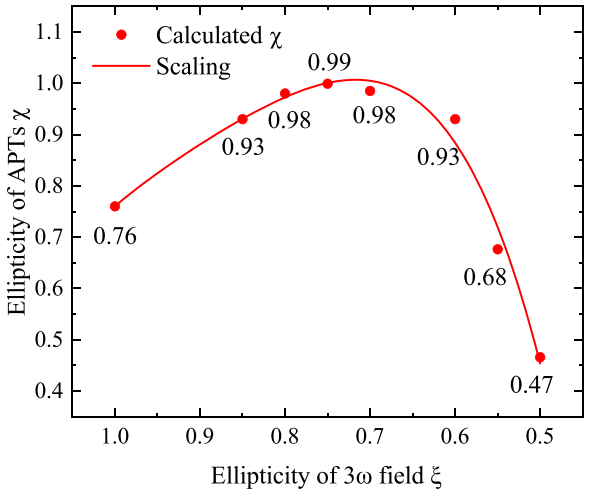

FIG. 4. The maximal ellipticity of the simulated attosecond pulse as a function of the ellipticity of the 3ω component of the ω-3ω circular-elliptical bichromatic laser field. The red curve is the result of a polynomial fit.

of the attosecond pulse first increases to approximately 0.99 and then starts to decline.

Note that we have also simulated the APTs with different frequency ranges of the harmonics in the HHG spectra and with different intensity ratios of the fundamental and additional fields. For the APTs synthesized with the harmonics in the lower-frequency region, e.g., 24th- to 30th-order harmonics, the ellipticity is almost unchanged with the decrease in the ellipticity of the driving laser fields. However, for the APTs synthesized with the harmonics in the higher-frequency region, e.g., 34th- to 44th-order harmonics, the ellipticities of the second and fourth attosecond bursts in each optical cycle first approach unity and then decrease as the ellipticity of the 3ω field decreases, which is qualitatively the same as the result shown in Fig. 4. On the other hand, we have also changed the ratios between the intensities of the fundamental and additional fields. Our results show that, for the different intensity ratios, the trend of the change in the attosecond bursts with the decrease of the ellipticity of the driving laser fields is quantitatively unchanged.

For comparison, in Figs. 3(g)–3(i), we show the APTs synthesized with the harmonics near the cutoff region for the ω-2ω circular-elliptical bichromatic laser field with different laser ellipticities ξ. Our result shows that there are three attosecond bursts in one optical cycle, and their polarization directions are 120° apart from each other, which is consistent with previous simulations [69]. With decreasing ellipticity ξ of the 2ω field, the APT changes significantly, but the ellipticity of the attosecond pulses is still small.

To understand the change in the ellipticity of the attosecond pulse under different circular-elliptical bichromatic laser fields, quantum-orbit theory within the SFA is employed to simulate the APTs. In Fig. 5, we present the simulated two-dimensional electric-field vectors of the APTs under different circular-elliptical bichromatic laser fields. Our simulations qualitatively agree with the TDSE results in Fig. 3. For example, for the ω-3ω circular-elliptical bichromatic laser field in Figs. 5(a)–5(c), the ellipticity of the attosecond burst with the main axis of the ellipse along the y direction increases with decreasing laser ellipticity ξ. This can be more clearly observed from the insets of Figs. 5(a)–5(c). On the other hand, for the ω-2ω circular-elliptical bichromatic laser field in Figs. 5(d)–5(f), the ellipticity of the attosecond burst remains small with decreasing laser ellipticity ξ.

In the following, we first understand the physics of the generation of the highly elliptically polarized attosecond pulse with the ω-3ω circular-elliptical bichromatic laser field by analyzing the harmonic amplitudes according to Eq. (10). In Fig. 6, we present the HHG spectra in the x and y directions at different laser ellipticities ξ. When $\xi = 1$, the harmonic amplitudes in the x and y directions are the same. With the decrease in the value of ξ, the high-energy harmonic amplitude in the y direction decreases significantly. If the APTs are synthesized with the high-energy harmonics, the decrease in the harmonic amplitude in the y direction leads to a decrease in the amplitude of the APTs in the y direction [see Figs. 5(a)–5(c)]. For the elliptically polarized attosecond pulses with the main axis of the ellipse along the y direction (the second and fourth attosecond bursts), the decrease in the amplitude of the APTs in the y direction results in the increase in the ellipticity of the corresponding attosecond pulses. At a proper ellipticity of the 3ω harmonic, it is possible to generate an attosecond pulse that is nearly circularly polarized.

Next, we will try to understand the change in the harmonic amplitudes in the different directions in Fig. 6 by analyzing the transition amplitude of the harmonic. According to Eq. (8), the harmonic amplitudes of the different directions are determined by the term $\sum_m \langle \Phi_{lm}|j|\boldsymbol{Q}_s\rangle$. For the He atom with $l = m = 0$, this term can be simplified as [73]

$$\begin{aligned}\langle \Phi_{00}|x|\boldsymbol{Q}_s\rangle = D Q_{s,x}\kappa^{-3-\nu}\Gamma(2+\nu)\Bigg\{&\sqrt{Q_{s,x}^2+Q_{s,y}^2}\,\kappa(1+\nu)\\ &\times\cos\Bigg[(1+\nu)\operatorname{arccot}\Bigg(\frac{\kappa}{\sqrt{Q_{s,x}^2+Q_{s,y}^2}}\Bigg)\Bigg]\\ &-\left[\kappa^2+Q_{s,x}^2(2+\nu)+Q_{s,y}^2(2+\nu)\right]\\ &\times\sin\Bigg[(1+\nu)\operatorname{arccot}\Bigg(\frac{\kappa}{\sqrt{Q_{s,x}^2+Q_{s,y}^2}}\Bigg)\Bigg]\Bigg\}\end{aligned} \tag{11}$$

in the x direction and

$$\begin{aligned}\langle \Phi_{00}|y|\boldsymbol{Q}_s\rangle = D Q_{s,y}\kappa^{-3-\nu}\Gamma(2+\nu)\Bigg\{&\sqrt{Q_{s,x}^2+Q_{s,y}^2}\,\kappa(1+\nu)\\ &\times\cos\Bigg[\Bigg(1+\nu)\operatorname{arccot}\Bigg(\frac{\kappa}{\sqrt{Q_{s,x}^2+Q_{s,y}^2}}\Bigg)\Bigg]\\ &-\left[\kappa^2+Q_{s,x}^2\Big(2+\nu\Big)+Q_{s,y}^2(2+\nu\right]\\ &\times\sin\Bigg[(1+\nu)\operatorname{arccot}\Bigg(\frac{\kappa}{\sqrt{Q_{s,x}^2+Q_{s,y}^2}}\Bigg)\Bigg]\Bigg\}\end{aligned} \tag{12}$$

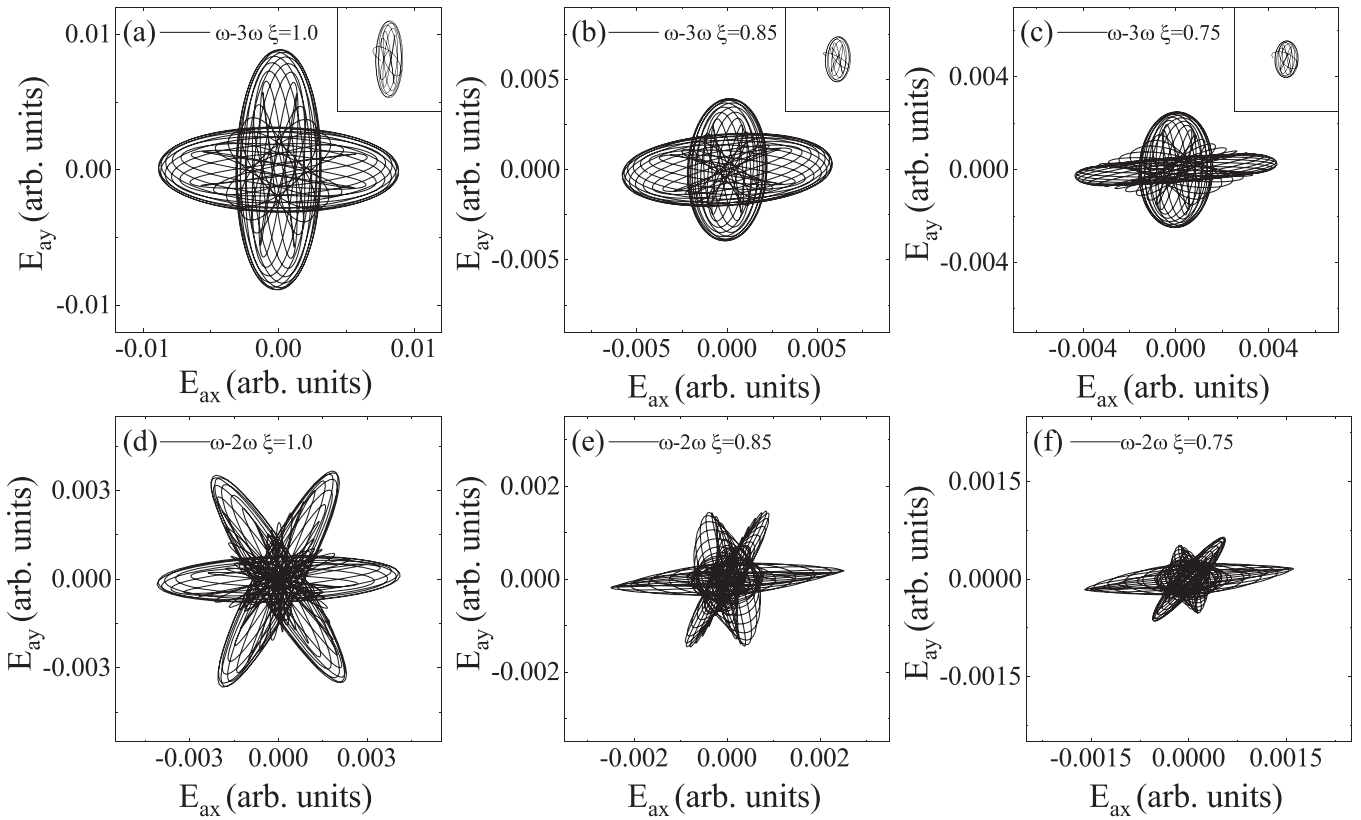

FIG. 5. The electric-field vector of the APTs simulated with quantum-orbit theory (a)–(c) for the ω-3ω circular-elliptical bichromatic laser field and (d)–(f) for the ω-2ω circular-elliptical bichromatic laser field. The electric vector is plotted by using the real part of Eq. (10). The insets of (a)–(c) are the results of the attosecond pulse for the temporal window of the 0.7–0.95 optical cycle of the fundamental laser field. The laser parameters are the same as those in Fig. 3.

in the y direction, where $D = -i\frac{2.87}{\sqrt{2}\pi(Q_{s,x}^2+Q_{s,y}^2)^{(3/2)}(1+\nu)}(1+\frac{Q_{s,x}^2+Q_{s,y}^2}{\kappa^2})^{\frac{1}{2}(-3-\nu)}$ and $Q_{s,j} = p_j + A_j(t_s)$ is the electron velocity at the recombination time. Close inspection reveals that the disparity between Eqs. (11) and (12) lies in the second term, i.e., the recombination velocity of the electron in the respective direction. In Fig. 7(a), we present the electron velocities of four short quantum orbits of, e.g., the 35th-order harmonic from the ionization time to the recombination time [59]. The recombination velocities of the quantum orbits from segments I and III (the black line and the medium gray line) are mainly along the y axis, which contributes to the harmonic in the y direction. On the other hand, the recombination velocities of the orbits from segments II and IV (the dark gray line and the light gray line) are mainly along the x direction, which contributes to the harmonic in the x direction. With decreasing

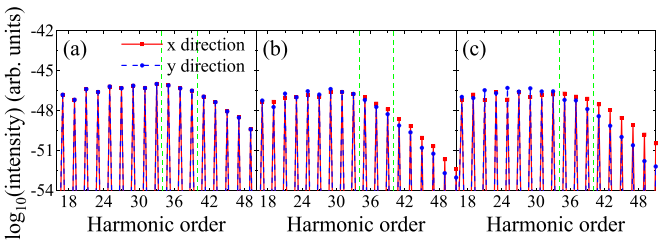

FIG. 6. The SFA HHG spectra of the ω-3ω circular-elliptical bichromatic laser field with (a) $\xi = 1$, (b) $\xi = 0.85$, and (c) $\xi = 0.75$. The red solid lines indicate the x-direction harmonics, while the blue dashed lines indicate the y-direction harmonics. The harmonics in the regions between the vertical green dashed lines are used to synthesize the APT.

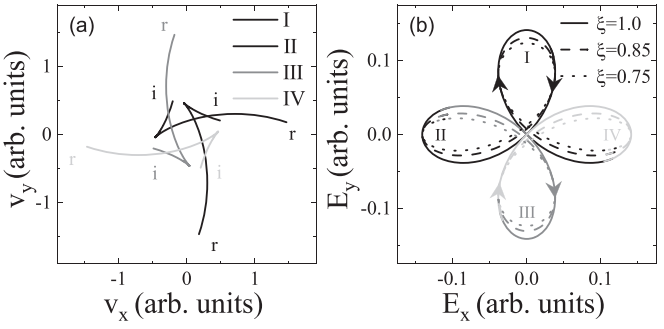

FIG. 7. (a) Velocities $\mathbf{v}(t)$ from the ionization time (i) to the recombination time (r) for the short quantum orbits of, e.g., the 35th-order harmonic under the ω-3ω bicircular laser field. The black line, dark gray line, medium gray line, and light gray line denote the quantum orbits from segments I, II, III, and IV, respectively. (b) Electric-field vectors of the ω-3ω circular-elliptical bichromatic laser field with $\xi = 1.0$, 0.85, and 0.75, respectively. The lines of varying colors are related to the travel times of the four quantum orbits from the ionization time to the recombination time.

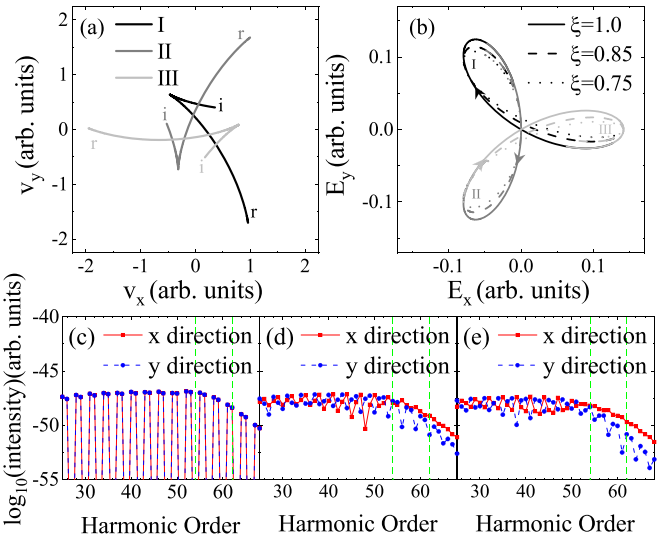

FIG. 8. (a) Velocities $\mathbf{v}(t)$ between the ionization time (i) and the recombination time (r) of the short quantum orbits of, e.g., the 59th-order harmonic from the ω-2ω bicircular laser field. The black line, dark gray line, and light gray line denote the quantum orbits from segments I, II, and III, respectively. (b) Electric-field vectors of the ω-2ω circular-elliptical bichromatic laser field. The lines of varying colors are related to the travel times of the three quantum orbits from the ionization time to the recombination time. (c)–(e) The HHG spectra in the x and y directions for the ω-2ω circular-elliptical bichromatic with $\xi = 1.0, 0.85, 0.75$, respectively.

ellipticity ξ of the 3ω field, Fig. 7(b) shows that the laser electric field along the y direction will gradually decrease, and accordingly, the maximal recombination velocities of the electron from segments I and III decrease, which results in the decrease in the cutoff energy of the harmonic in the y direction. However, the electric field in the x direction remains almost the same, and hence, the change in the harmonic amplitude in the x direction with the ellipticity ξ of the 3ω field is relatively small.

Finally, we will try to understand the change in the APTs under the ω-2ω circular-elliptical bichromatic laser fields shown in Figs. 5(d)–5(f). Similarly, in Fig. 8(a), we present the electron velocities of three short quantum orbits of, e.g., the 59th-order harmonic from the ionization time to the recombination time. For the quantum orbit from segment III, the direction of the velocity at the recombination time is mainly along the x direction, and for the quantum orbits from segments I and II, their velocities at the recombination time are not along the x or y axis. According to the discussion above, the direction of the electron recombination velocity determines the polarization direction of the harmonic emission. Thus, the polarization directions of the synthesized attosecond pulse are 120° apart from each other. With decreasing ellipticity ξ of the 2ω laser field, Fig. 8(b) shows that the laser electric field along the y direction will gradually decrease, while the electric field in the x direction remains almost the same. Therefore, the harmonic amplitude in the y direction decreases significantly in comparison with that in the x direction, which is in good agreement with the simulations shown in Figs. 8(c)–8(e). The decrease in the harmonic amplitude in the y direction results in a corresponding decrease in the amplitude of the attosecond pulse in the same direction. However, it is important to note that unlike the ω-3ω circular-elliptical bichromatic laser field, the main axis of the elliptically polarized attosecond pulse is not aligned with the y direction [see Fig. 5(d)]. Consequently, the reduction in the attosecond pulse amplitude along the y direction leads to a significant decrease in its ellipticity, as depicted in Figs. 5(d)–5(f).

IV. CONCLUSION

In summary, we investigated the generation of APT from an atom under circular-elliptical bichromatic laser fields by numerically solving the TDSE. With decreasing ellipticity of the 3ω field, in $\omega - 3\omega$ circular-elliptical bichromatic laser field the ellipticity of parts of the elliptically polarized APT in each optical cycle first approaches unity and then decreases. However, the ellipticity of the attosecond pulses remains small when the ellipticity of the 2ω field in $\omega - 2\omega$ circular-elliptical bichromatic laser field is unchanged. The TDSE results were reproduced in terms of quantum-orbit theory. By analyzing the quantum orbits, we found that the harmonic amplitude emitted in the different directions is closely related to the electron velocity at the recombination time and hence the laser electric field in the corresponding direction. For the ω-3ω circular-elliptical bichromatic laser field, the electric field decreases just along the main axis of the elliptically polarized attosecond pulse, leading to a decrease in the amplitude of the attosecond pulses in that direction. Hence, the ellipticity of the attosecond pulses first approaches unity and then decreases. Our work offers a simple method to obtain highly elliptically polarized attosecond pulses by controlling the electric field of circular-elliptical bichromatic laser fields.

ACKNOWLEDGMENTS

This work was supported by the National Key Program for S&T Research and Development (Grant No. 2019YFA0307702), the National Natural Science Foundation of China (Grants No. 11834015, No. 11922413, No. 12121004, No. 12274420, No. U21A20435, and No. 92265206), and the CAS Project for Young Scientists in Basic Research (Grant No. YSBR-055).

[1] M. Hentschel, R. Kienberger, Ch. Spielmann, G. A. Reider, N. Milosevic, T. Brabec, P. Corkum, U. Heinzmann, M. Drescher, and F. Krausz, Nature (London) **414**, 509 (2001).

[2] F. Kelkensberg, W. Siu, J. F. Pérez-Torres, F. Morales, G. Gademann, A. Rouzée, P. Johnsson, M. Lucchini, F. Calegari, J. L. Sanz-Vicario, F. Martín, and M. J. J. Vrakking, Phys. Rev. Lett. **107**, 043002 (2011).

[3] P. Lan, M. Ruhmann, L. He, C. Zhai, F. Wang, X. Zhu, Q. Zhang, Y. Zhou, M. Li, M. Lein, and P. Lu, Phys. Rev. Lett. **119**, 033201 (2017).

[4] B. Bergues, M. Kübel, N. G. Johnson, B. Fischer, N. Camus, K. J. Betsch, O. Herrwerth, A. Senftleben, A. M. Sayler, T. Rathje, T. Pfeifer, I. BenItzhak, R. R. Jones, G. G. Paulus, F. Krausz, R. Moshammer, J. Ullrich, and M. F. Kling, Nat. Commun. **3**, 813 (2012).

[5] X. Shi, C. T. Liao, Z. Tao, E. Cating-Subramanian, M. M. Murnane, C. Hernández-Garcíaand, and H. C. Kapteyn, J. Phys. B **53**, 184008 (2020).

[6] G. Farkas and C. Tóth, Phys. Lett. A **168**, 447 (1992).

[7] R. Kienberger, E. Goulielmakis, M. Uiberacker, A. Baltuska, V. Yakovlev, F. Bammer, A. Scrinzi, Th. Westerwalbesloh, U. Kleineberg, U. Heinzmann, M. Drescher, and F. Krausz, Nature (London) **427**, 817 (2004).

[8] H. Y. Zhong, J. Guo, H. D. Zhang, H. Du, and X. S. Liu, Chin. Phys. B **24**, 073202 (2015).

[9] H. Du, L. Luo, X. Wang, and B. Hu, Opt. Express **20**, 9713 (2012).

[10] C. L. Xia, Q. Y. Liu, and X. Y. Miao, Opt. Commun. **407**, 127 (2018).

[11] P. B. Corkum, Phys. Rev. Lett. **71**, 1994 (1993).

[12] K. J. Schafer, B. Yang, L. F. DiMauro, and K. C. Kulander, Phys. Rev. Lett. **70**, 1599 (1993).

[13] P. Antoine, A. L'Huillier, and M. Lewenstein, Phys. Rev. Lett. **77**, 1234 (1996).

[14] A. D. Bandrauk, S. Chelkowski, S. Kawai, and H. Lu, Phys. Rev. Lett. **101**, 153901 (2008).

[15] J. Li, X. Ren, Y. Yin, K. Zhao, A. Chew, Y. Cheng, E. Cunningham, Y. Wang, S. Hu, Y. Wu, M. Chini, and Z. Chang, Nat. Commun. **8**, 186 (2017).

[16] T. S. Sarantseva, M. V. Frolov, N. L. Manakov, A. A. Silaev, A. A. Romanov, N. V. Vvedenskii, and A. F. Starace, Phys. Rev. A **101**, 013402 (2020).

[17] E. Goulielmakis, M. Schultze, M. Hofstetter, V. S. Yakovlev, J. Gagnon, M. Uiberacker, A. L. Aquila, E. M. Gullikson, D. T. Attwood, R. Kienberger, F. Krausz, and U. Kleineberg, Science **320**, 1614 (2008).

[18] T. Gaumnitz, A. Jain, Y. Pertot, M. Huppert, I. Jordan, F. Ardana-Lamas, and H. J. Worner, Opt. Express **25**, 27506 (2017).

[19] G. Sansone, E. Benedetti, F. Calegari, C. Vozzi, L. Avaldi, R. Flammini, L. Poletto, P. Villoresi, C. Altucci, R. Velotta, S. Stagira, S. D. Silvestri, and M. Nisoli, Science **314**, 443 (2006).

[20] N. Böwering, T. Lischke, B. Schmidtke, N. Müller, T. Khalil, and U. Heinzmann, Phys. Rev. Lett. **86**, 1187 (2001).

[21] U. Hergenhahn, E. E. Rennie, O. Kugeler, S. Marburger, T. Lischke, I. Powis, and G. Garcia, J. Chem. Phys. **120**, 4553 (2004).

[22] R. Cireasa, A. E. Boguslavskiy, B. Pons, M. C. H. Wong, D. Descamps, S. Petit, H. Ruf, N. Thire, A. Ferre, J. Suarez, J. Higuet, B. E. Schmidt, A. F. Alharbi, F. Legare, V. Blanchet, B. Fabre, S. Patchkovskii, O. Smirnova, Y. Mairesse, and V. R. Bhardwaj, Nat. Phys. **11**, 654 (2015).

[23] S. Beaulieu, A. Comby, B. Fabre, D. Descamps, A. Ferre, G. Garcia, R. Geneaux, F. Legare, L. Nahon, S. Petit, T. Ruchon, B. Pons, V. Blanchet, and Y. Mairesse, Faraday Discuss. **194**, 325 (2016).

[24] O. Neufeld and O. Cohen, Phys. Rev. Lett. **120**, 133206 (2018).

[25] G. Hu, X. Hong, K. Wang, J. Wu, H. X. Xu, W. Zhao, W. Liu, S. Zhang, F. Garcia-Vidal, B. Wang, P. Lu, and C. W. Qiu, Nat. Photonics **13**, 467 (2019).

[26] T. Fan *et al.*, Proc. Natl. Acad. Sci. USA **112**, 14206 (2015).

[27] F. Siegrist, J. A. Gessner, M. Ossiander, C. Denker, Y. P. Chang, M. C. Schröder, A. Guggenmos, Y. Cui, J. Walowski, U. Martens, J. K. Dewhurst, U. Kleineberg, M. Münzenberg, S. Sharma, and M. Schultze, Nature (London) **571**, 240 (2019).

[28] C. Boeglin, E. Beaurepaire, V. Halte, V. Lopez-Flores, C. Stamm, N. Pontius, H. A. Durr, and J. Y. Bigot, Nature (London) **465**, 458 (2010).

[29] C. D. Stanciu, F. Hansteen, A. V. Kimel, A. Kirilyuk, A. Tsukamoto, A. Itoh, and T. Rasing, Phys. Rev. Lett. **99**, 047601 (2007).

[30] I. Barth and O. Smirnova, J. Phys. B **47**, 204020 (2014).

[31] H. Eichmann, A. Egbert, S. Nolte, C. Momma, B. Wellegehausen, W. Becker, S. Long, and J. K. McIver, Phys. Rev. A **51**, R3414 (1995).

[32] S. Long, W. Becker, and J. K. McIver, Phys. Rev. A **52**, 2262 (1995).

[33] T. Zuo and A. D. Bandrauk, J. Nonlinear Opt. Phys. Mater. **4**, 533 (1995).

[34] D. B. Milošević, J. Phys. B **48**, 171001 (2015).

[35] S. Odžak and D. B. Milošević, Phys. Rev. A **92**, 053416 (2015).

[36] O. Kfir, P. Grychtol, E. Turgut, R. Knut, D. Zusin, D. Popmintchev, T. Popmintchev, H. Nembach, J. M. Shaw, A. Fleischer, H. Kapteyn, M. Murnane, and O. Cohen, Nat. Photonics **9**, 99 (2015).

[37] A. Fleischer, O. Kfir, T. Diskin, P. Sidorenko, and O. Cohen, Nat. Photonics **8**, 543 (2014).

[38] M. V. Frolov, N. L. Manakov, A. A. Minina, N. V. Vvedenskii, A. A. Silaev, M. Yu. Ivanov, and A. F. Starace, Phys. Rev. Lett. **120**, 263203 (2018).

[39] C. Chen, Z. Tao, C. Hernández-García, P. Matyba, A. Carr, R. Knut, O. Kifr, D. Zusin, C. Gentry, P. Grychtol, O. Cohen, L. Plaja, A. Becker, A. Jaron-Becker, H. Kapteyn, and M. Murnane, Sci. Adv. **2**, e1501333 (2016).

[40] L. Medišauskas, J. Wragg, H. van der Hart, and M. Yu. Ivanov, Phys. Rev. Lett. **115**, 153001 (2015).

[41] D. B. Milošević, Opt. Lett. **40**, 2381 (2015).

[42] C. L. Xia, Y. Y. Lan, Q. Q. Li, and X. Y. Miao, Chin. Phys. B **28**, 103203 (2019).

[43] D. B. Milošević, Phys. Rev. A **92**, 043827 (2015).

[44] K. M. Dorney, J. L. Ellis, C. Hernández-García, D. D. Hickstein, C. A. Mancuso, N. Brooks, T. Fan, G. Fan, D. Zusin, C. Gentry, P. Grychtol, H. C. Kapteyn, and M. M. Murnane, Phys. Rev. Lett. **119**, 063201 (2017).

[45] Á. Jiménez-Galán, N. Zhavoronkov, D. Ayuso, F. Morales, S. Patchkovskii, M. Schloz, E. Pisanty, O. Smirnova, and M. Ivanov, Phys. Rev. A **97**, 023409 (2018).

[46] D. B. Milošević, Phys. Rev. A **98**, 033405 (2018).

[47] R. Shao, C. Zhai, Y. Zhang, N. Sun, W. Cao, P. Lan, and P. Lu, Opt. Express **28**, 15874 (2020).

[48] H. Yuan, L. He, S. M. Njoroge, D. Wang, R. Shao, P. Lan, and P. Lu, Ann. Phys. (Berlin, Ger.) **532**, 1900570 (2020).

[49] T. S. Sarantseva, A. A. Romanov, A. A. Silaev, N. V. Vvedenskii, and M. V. Frolov, Phys. Rev. A **107**, 023113 (2023).

[50] A. Weber, B. Böning, B. Minneker, and S. Fritzsche, Phys. Rev. A **104**, 063118 (2021).

[51] M. F. Zhu, G. L. Wang, S. F. Zhao, X. Y. Li, and X. X. Zhou, J. Mod. Opt. **66**, 1467 (2019).

[52] R. Rajpoot, A. R. Holkundkar, and J. N. Bandyopadhyay, J. Phys. B **54**, 225401 (2021).
[53] V. Tulsky and D. Bauer, Comput. Phys. Commun. **251**, 107098 (2020).
[54] X. M. Tong and C. D. Lin, J. Phys. B **38**, 2593 (2005).
[55] A. D. Bandrauk, S. Chelkowski, D. J. Diestler, J. Manz, and K. J. Yuan, Phys. Rev. A **79**, 023403 (2009).
[56] K. Burnett, V. C. Reed, J. Cooper, and P. L. Knight, Phys. Rev. A **45**, 3347 (1992).
[57] P. C. Li, I. L. Liu, and S. I. Chu, Opt. Express **19**, 23857 (2011).
[58] M. Lewenstein, Ph. Balcou, M. Yu. Ivanov, A. L'Huillier, and P. B. Corkum, Phys. Rev. A **49**, 2117 (1994).
[59] D. B. Milošević, J. Mod. Opt. **66**, 47 (2019).
[60] S. Odžak and D. B. Milošević, Phys. Rev. A **72**, 033407 (2005).
[61] D. B. Milošević and W. Becker, Phys. Rev. A **93**, 063418 (2016).
[62] D. B. Milošević, G. G. Paulus, D. Bauer, and W. Becker, J. Phys. B **39**, R203 (2006).
[63] A. A. Radzig and B. M. Smirnov, *Reference Data on Atoms, Molecules and Ions* (Springer, Berlin, 1985).
[64] G. F. Gribakin and M. Y. Kuchiev, Phys. Rev. A **55**, 3760 (1997).
[65] D. B. Milošević, A. Gazibegović-Busuladžić, and W. Becker, Phys. Rev. A **68**, 050702(R) (2003).
[66] A. Gazibegović-Busuladžić, D. B. Milošević, and W. Becker, Phys. Rev. A **70**, 053403 (2004).
[67] D. B. Milošević and W. Becker, Phys. Rev. A **66**, 063417 (2002).
[68] D. B. Milošević, E. Hasović, M. Busuladžić, A. Gazibegović-Busuladžić, and W. Becker, Phys. Rev. A **76**, 053410 (2007).
[69] D. B. Milošević and W. Becker, Phys. Rev. A **62**, 011403(R) (2000).
[70] Z. Y. Chen, Phys. Rev. E **97**, 043202 (2018).
[71] E. Pisanty, S. Sukiasyan, and M. Ivanov, Phys. Rev. A **90**, 043829 (2014).
[72] D. B. Milošević, W. Becker, and R. Kopold, Phys. Rev. A **61**, 063403 (2000).
[73] S. Odžak and D. B. Milošević, Phys. Rev. A **79**, 023414 (2009).